Annals of Botany **120**: 693–708, 2017
doi:10.1093/aob/mcx050, available online at www.academic.oup.com/aob

ANNALS OF BOTANY
Founded 1887

PART OF A SPECIAL ISSUE ON MORPHOLOGY AND ADAPTATION

Cell wall changes during the formation of aerenchyma in sugarcane roots

D. C. C. Leite[1,#], A. Grandis[1,#], E. Q. P. Tavares[1], A. R. Piovezani[1], S. Pattathil[2], U. Avci[2], A. Rossini, A. Cambler[1], A. P. De Souza[1,†], M. G. Hahn[2] and M. S. Buckeridge[1]*

[1]Laboratory of Plant Physiological Ecology (LAFIECO), Department of Botany, Institute of Biosciences, University of São Paulo, Rua do Matão 277, Sao Paulo, SP, Brazil and [2]BioEnergy Science Center, Complex Carbohydrate Research Center, The University of Georgia, 315 Riverbend Road, Athens, GA 30602, USA
**For correspondence. E-mail msbuck@usp.br*
[†]Present address: Carl R. Woese Institute for Genomic Biology, University of Illinois at Urbana-Champaign, Urbana, IL 61801, USA.
[#]These two authors contributed equally to this work.

Received: 10 January 2017 Returned for revision: 28 February 2017 Editorial decision: 10 March 2017 Accepted: 5 April 2017
Published electronically: 4 July 2017

• **Background and Aims** Aerenchyma develops in different plant organs and leads to the formation of intercellular spaces that can be used by the plant to transport volatile substances. Little is known about the role of cell walls in this process, although the mechanism of aerenchyma formation is known to involve programmed cell death and some cell wall modifications. We assessed the role that cell wall-related mechanisms might play in the formation of aerenchyma in sugarcane roots.
• **Methods** Sections of roots (5 cm) were subjected to microtomography analysis. These roots were divided into 1-cm segments and subjected to cell wall fractionation. We performed analyses of monosaccharides, oligosaccharides and lignin and glycome profiling. Sections were visualized by immunofluorescence and immunogold labelling using selected monoclonal antibodies against polysaccharide epitopes according to the glycome profiles.
• **Key Results** During aerenchyma formation, gas spaces occupied up to 40 % of the cortex cross-section within the first 5 cm of the root. As some of the cortex cells underwent dissolution of the middle lamellae, leading to cell separation, cell expansion took place along with cell death. Mixed-linkage β-glucan was degraded along with some homogalacturonan and galactan, culminating in the formation of cell wall composites made of xyloglucan, arabinoxylans, cellulose and possibly lignin.
• **Conclusion** The composites formed seem to play a role in the physical–chemical properties of the gas chambers, providing mechanical resistance to forces acting upon the root and at the same time decreasing permeability to gases.

Key words: Aerenchyma, cell wall, pectin, hemicellulose, cellulose, arabinoxylan, xyloglucan, β-glucan, glycome profile, bioenergy, *Saccharum.*

INTRODUCTION

The aerenchyma is a tissue that comprises a set of interconnected air chambers with larger gaps than those found in intercellular spaces (Evans, 2003). It may occur in petioles, stems and roots as part of development. In this case it is called constitutive aerenchyma. This type of aerenchyma has been described in many wetland species, such as *Juncus effusus*, *Spartina patens*, some varieties of rice and at least one maize relative (Justin and Armstrong, 1991; Schussler and Longstreth, 2000; Visser and Bögelman, 2006; Abiko *et al*., 2012).

Environmental and endogenous conditions can also trigger aerenchyma formation; in this case the tissue is called induced aerenchyma (Evans, 2003). Most aerenchyma research focuses on this induced form, more precisely in maize roots, even though it also takes place in crops like barley, wheat, soybean and bean (Yamauchi *et al*., 2013).

The process leading to aerenchyma formation (constitutive or induced) can be lysigenous, schizogenous or expansigenous (Evans, 2003; Seago *et al*., 2005). In the first case, cell wall separation results from lysis associated with programmed cell death. Rapidly increasing levels of ethylene trigger the latter, which usually occurs as a response to hypoxia in waterlogged environments (He *et al*., 1996). The onset of programmed cell death occurs through soil compaction (Drew *et al*., 2000) or due to increased ethylene sensitivity as a consequence of nutritional starvation (He *et al*., 1994). The ethylene signalling cascade induces cellular ultrastructural changes such as plasma membrane invagination and shrinkage, an increase in electron density of cytoplasm and DNA cleavage. At the same time, the activation of cell wall modifications takes place (Gunawardena *et al*., 2001*a*; Rajhi *et al*., 2011) and some studies suggest complete cell wall degradation during lysigenous aerenchyma formation (Kawase, 1979; Gunawardena *et al*., 2001*b*).

Aerenchyma formation correlates with the rise in glycosyl hydrolase activities and related mRNA accumulation while cell wall changes are taking place. The suggestion that there is degradation of cellulose and xylan during programmed cell death has been supported by the detection of endo-β-glucanase (He *et al*., 1994, 1996) and endo-β-xylanase (Bragina *et al*., 2001) activities during aerenchyma formation.

Xyloglucans may also be a target for changes during aerenchyma development, since the induction of transcripts of

xyloglucan transglycosylase-hydrolase has been detected in flooded maize roots (Saab and Sachs, 1996; Rajhi *et al*., 2011).

Using a combination of laser microdissection and microarray analyses in maize roots under waterlogging or treated with 1-methylcyclepropene (1-MCP; a known ethylene perception inhibitor), Rajhi *et al*. (2011) found that endopolygalacturonase and cellulase genes were differentially expressed, seeming to be directly associated with the phenomenon of aerenchyma formation.

Begum *et al*. (2013) found that all sugarcane roots form aerenchyma, except for those from aerial nodes. In their observations, the formation of aerenchyma was independent of flooding. Tetsushi and Karim (2007) described aerenchyma formation in a series of sugarcane varieties and suggested that its formation is constitutive in that plant.

The composition and fine structure of sugarcane cell walls from leaves and culm, but not from roots, have been characterized recently (De Souza *et al*., 2013). Sugar cane walls consist of cellulose, which accounts for 28 % of the wall, and hemicelluloses that are thought to be strongly and weakly bonded cellulose; these hemicelluloses consist mostly of arabinoxylan (40 %), β-glucan (10 %) and xyloglucan (8 %). These polysaccharides are embedded in a thin pectin matrix (8 %) composed of homogalacturonan and rhamnogalacturonans branched with arabinogalactans.

Cell wall architecture is complex and requires many enzymes for its degradation. Understanding how the plant can degrade its cell walls in a carefully regulated manner, as seems to occur in aerenchyma formation in sugarcane roots, may provide information that will be valuable in the development of methods to access cell walls in order to generate new technologies for the production of biofuels (Grandis *et al*., 2014).

In this work we studied for the first time the dynamics of cell wall composition in roots of sugarcane during aerenchyma formation and found that the biochemical modifications are not consistent with complete cell wall degradation. Cell wall events include cell separation, hemicellulose (β-glucan) degradation and the formation of a cell wall composite made of hemicelluloses, cellulose and possibly lignin. We discuss the cell wall changes in the light of possible applications in biotechnology.

MATERIALS AND METHODS

Plant material and growth conditions

The sugarcane variety used in this work was SP80-3280. We cultivated cuttings (single-node culm sets containing one vegetative bud) in trays containing dampened vermiculite medium in a greenhouse for 15 d. We selected plantlets with uniform shoots and planted them in 10-L pots containing vermiculite. They were kept under natural environmental conditions for 90 d (from April to June in 2011 and 2012, with average temperature 26 °C). Fertilizer (NPK 30:20:30) was added to the starting medium. Pots were watered every 2 d. There was no detection of visible symptoms of water or nutritional stress during the experiments. After sampling, we washed the tiller roots in running tap water and then rinsed them with distilled water. Part of the samples were frozen in liquid nitrogen and liofilized and another part was fixed for microscopy analyses.

Light microscopy and aerenchyma quantification

We divided roots from seven plants into 1-cm segments (0–1, 1–2, 2–3, 3–4 and 4–5 cm from the root apex, hereafter called segments S1, S2, S3, S4 and S5, respectively) and preserved them in 70 % ethanol for 24 h. The segments were transferred to 50 % ethanol and subjected to an ethanol/butanol series (50, 70, 85, 95 and 100 % v/v butanol) for 2 h in each step, followed by incubation in 100 % butanol overnight, before embedding them in paraffin wax. Sections (12 μm) were obtained using a Leica RM2145 microtome, mounted on glass slides and stained with astra blue and safranin (1 % of each).

For observation of the sections, we used an Olympus BX51 microscope. We captured images with an Olympus Evolt E-330 digital camera. The percentage area of aerenchyma in the cortex was estimated using Image-Pro software (MediaCybernetics, v.6.3).

X-ray microtomography

Microtomography was performed with fresh root sections, 5 cm long, in a high-performance *in vivo* micro-CT scanner (Skyscan 1176). The number of images obtained was 2970 (pixel size 17·4 μm). The volume of aerenchyma was determined from 2970 images (pixel size of 17.4 μm) using the software CT-Analyser v.1.13 (Bruker-microCT, 2013). The number of voxels from the regions corresponding to segments S1 to S5 were used to calculate the percentage of aerenchyma.

X-ray microtomography was used to study the disposition of gas spaces in the cortex along the aerenchyma, and a video of a 5-cm section is shown in Supplementary Data Video.

Cell wall fractionation

Biochemical analyses were conducted separately in root segments (S1–S5) with five replicates. Each sample had segments from ten plants. We ground the lyophilized samples in liquid nitrogen. Soluble sugars were extracted six times with 80 % ethanol at 80 °C for 20 min. Alcohol-insoluble residues of the sections were fractionated by the procedure described by De Souza *et al*. (2013). The alcohol-insoluble residues of each sample were extracted with 490 mM sodium chlorite in 0·3 % acetic acid for 1 h at 65 °C followed by an extraction with 0·5 % ammonium oxalate for 3 h at 80 °C. We subjected the pellets to sequential extraction (1 h each) with NaOH (0·1, 1 and 4 M) containing $NaBH_4$ (3 mg mL^{-1}) at room temperature. After each step, the materials were pelleted by centrifugation (3220 *g* for 20 min) and washed with distilled water five times before addition of the next solution. Supernatants were neutralized using glacial acetic acid, dialysed and freeze-dried for subsequent analyses.

Determination of lignin

We performed lignin quantification in two steps: (1) removal of proteins from the cell wall and (2) extraction of lignin from the cell wall without proteins. These steps were executed according to Moreira-Vilar *et al*. (2014). To obtain a cell wall free of proteins, 20 mg of dry mass from each segment was

homogenized in 50 mM potassium phosphate buffer and washed successively with 1 % Triton X-100, 1 M sodium chloride and twice with pure acetone. We washed the samples with water and dried them at 45 °C. One milligram of each sample was suspended in 25 % acetyl bromide in acetic acid and incubated at 70 °C for 30 min. Two hundred microlitres of a solution containing 1·5 M sodium hydroxide, 0·5 M hydroxylamine hydrochloride and glacial acetic acid were added to the mixture. After centrifugation (1400 *g* for 5 min), the absorbance of the supernatant was measured at 280 nm, revealing the lignin content.

Monosaccharide profile

Two milligrams of each cell wall fraction was hydrolysed with 100 µL of 72 % sulphuric acid (v/v) for 45 min at 30 °C. The solution was diluted to 4 % with deionized water and autoclaved for 1 h at 120 °C (Saeman *et al*., 1945). Samples were neutralized with NaOH and deionized through cation and anion exchange columns (Dowex®). The neutral monosaccharide composition was determined by high-performance anion exchange chromatography with pulsed amperometric detection (HPAEC/PAD) in a Dionex DX-500 system using a Carbo-Pac SA10 column. Monosaccharides were separated isocratically in a 1.2 mM NaOH solution with a flow rate of 1 mL min^{-1}. We used a post-column base containing 500 mM NaOH with a flow rate of 0·5 mL min^{-1} to produce the alkaline conditions necessary for detection by PAD (De Souza *et al*., 2013).

Oligosaccharide analysis

Oligosaccharide analysis was performed according to De Souza *et al*. (2013). Fractions were solubilized to 1 % (w/v) in 50 mM sodium acetate buffer, pH 5, and used as substrates in incubations with 0·5 U of the following enzymes: (1) lichenase (Megazyme®); (2) endo-β-xylanase (Sigma®); and (3) GH12 or xyloglucan endoglucanase (XEG; purified according to Damásio *et al*., 2012). Incubations were performed at pH 5 (50 mM ammonium acetate buffer) for 24 h at 30 °C to assess the fine structure of β-glucans, xylans and xyloglucans, respectively. After incubation, samples were filtered using a Millipore filter (20 µm mesh) and subsequently analysed by HPEAC/PAD (Dionex ICS-3000 system). We used a CarboPac PA-100 column with 88 mM NaOH and 200 mM sodium acetate as eluent (flow rate 0·9 mL min^{-1}) for 45 min (De Souza *et al*., 2013).

Glycome profiling

Glycome profiling of the cell wall fractions of all roots segments was performed as described by Pattathil *et al*. (2012). The technique consists of an ELISA screening of extracts of cell wall fractions with a comprehensive library of cell wall glycan-directed monoclonal antibodies (Zhu *et al*., 2010; Demartini *et al*., 2011; Kong *et al*., 2011; Pattathil *et al*., 2012; De Souza *et al*., 2015). The results are shown as a heat map, being the average of five replicates composed of samples of roots of 10 different individuals in each replicate of every cell wall fraction from each segment.

Immunofluorescence labelling

Segments from fresh tissue were fixed in 1·6 % (v/v) paraformaldehyde and 0·2 % (v/v) glutaraldehyde in 25 mM sodium phosphate buffer, pH 7.1. Embedding, sectioning and immunolabelling were performed as described by Pattathil *et al*. (2010) and Avci *et al*. (2012). Sections rendered no autofluorescence unless magnifications were higher than ×100.

The monoclonal antibodies used were CCRC-M95 (non-fucosylated xyloglucan), CCRC-M84 (fucosylated xyloglucan), CCRC-M138 (xylan-6 - xylan backbone, DP > 5), CCRC-M154 (xylan-4 - arabinoxylan), BG1 (β-glucan), CCRC-M38 (de-esterified homogalacturonan backbone, DP > 4), JIM14 and JIM19 (arabinogalactans) and CCRC-M80 (rhamnogalacturonan-I/arabinogalactan). We applied Citifluor antifade mounting medium AF1 (Electron Microscopy Sciences) before placing a coverslip. Images were captured with a Nikon Eclipse 80i microscope with a Nikon DS-Ri1 camera head using NIS-Elements Basic Research software.

Transmission electron microscopy and immunolocalization with colloidal gold

Immunolocalizations were carried out using selected cell wall glycan-directed monoclonal antibodies followed by fluorescence microscopy (see above). In all cases, we prepared negative controls without the secondary antibodies.

For transmission electron microscopy (TEM) analyses, we embedded materials in LR white resin. Sections (80 nm) were obtained using a Leica EM UC6 microtome. They were stained with 2 % uranyl acetate for 5 min and Reynolds lead citrate for 1 min.

Immunolocalizations were carried out using selected cell wall glycan-directed monoclonal antibodies followed by addition of the secondary antibody conjugated with colloidal gold to root segments S4 and S5. Sections (80 nm) were incubated in 5 % bovine serum albumin (BSA) in 10 mM phosphate-buffered saline (KPBS) for 30 min. The sections were incubated for 1 h with antibodies CCRC-M154, BG1 and CCRC-M38, followed by washing with 10 mM KPBS for 30 s. Sections were incubated with the secondary antibody Alexa Fluor 488 anti-mouse immunoglobulin G, conjugated to 15 nm colloidal gold diluted 1:10 in 10 mM KPBS. The sections were washed for 30 s in KPBS and distilled water.

Sections used for colloidal immunogold localization were observed in a transmission electron microscope (Zeiss 902A), whereas sections used for observation of cell wall structures were observed in a Zeiss EM900 microscope. Both were operated at 80 kV. To facilitate visualization of the gold particles, they were digitally coloured in red. Original figures showing colloidal gold staining are shown in Supplementary Data Fig. S5.

Statistical analysis

The percentage of aerenchyma formation (% of tissue that form aerenchyma within the cross-section of the root in each segment), monosaccharides and glycome profile were analysed using the software JMP 5.0.1 (©1989-2002 SAS Institute Inc.). The homogeneity of variance was tested and one-way

parametric analysis of variance (ANOVA) was performed, followed by the *a posteriori* Tukey test ($P < 0{\cdot}05$).

RESULTS

Aerenchyma development in sugarcane

We noticed the first signs of gas spaces in S2 (labelled 'a' in Fig. 1C) in the form of a few enlarged intercellular spaces. The fully developed aerenchyma was visualized in S5 (i.e. 5 cm from the apex; Fig. 1F). In this segment aerenchyma occupied, on average, 37 % of the cortex. At the end of aerenchyma development, we visualized radial compartments separated by chains of intact cells (labelled 'b' in Fig. 1F) or collapsed walls forming gas spaces (arrows in inserts in Fig. 1E, F). Aerenchyma was fully developed beyond 5 cm from the root tip and towards the root basis in all samples analysed, similarly to S5 (data not shown). Aerenchyma develops centripetally, initially by changes in the walls of the peripheral cells of the cortex. It continues to develop towards the vascular cylinder (arrows in Fig. 1E, F).

The Supplementary Data Video permits visualization of each segment of the aerenchyma using microtomography. Gas spaces inside the root can be seen in S2 and become more evident from S3 onwards. The video shows the centripetal disposition of the aerenchyma and regions where aerenchyma almost completely fills the cortex in S5. However, the video shows that chambers filling the cortex section completely are only rarely observed. Calculated on the basis of voxels obtained from the microtomographic digital images, the volume of the fully formed aerenchyma was ~40 % of the whole tissue, matching the calculations made from the microscopic sections.

Cell wall fractionation yield and lignin content

The mass recovery in each cell wall fraction differed along the root segments (Fig. 2). Segment S1 differed from segments S2–S5 as the yields in sodium chlorite and ammonium oxalate fractions were significantly higher. The NaOH fractions displayed relatively low yields (10–15 %), whereas the final residues after all extractions were higher (35–45 %) for S2–S5. It seems that the residual fractions of these segments are mostly composed of cellulose since glucose composition was >96 % in all of them (Table 1). The increase in cellulose observed from S1 to S5 was probably associated with secondary wall formation in the vascular cylinder.

The percentage of lignin did not vary significantly among the segments, averaging between 5 and 9 % of the dry weight of the segments (Supplementary Data Fig. S4), indicating that there is little lignification of the walls in the first 5 cm of the root.

Monosaccharide profile

Table 1 shows the monosaccharide composition of cell wall fractions from S1 to S5. Polymers from the sodium chlorite fraction were composed mainly of arabinose, galactose, glucose

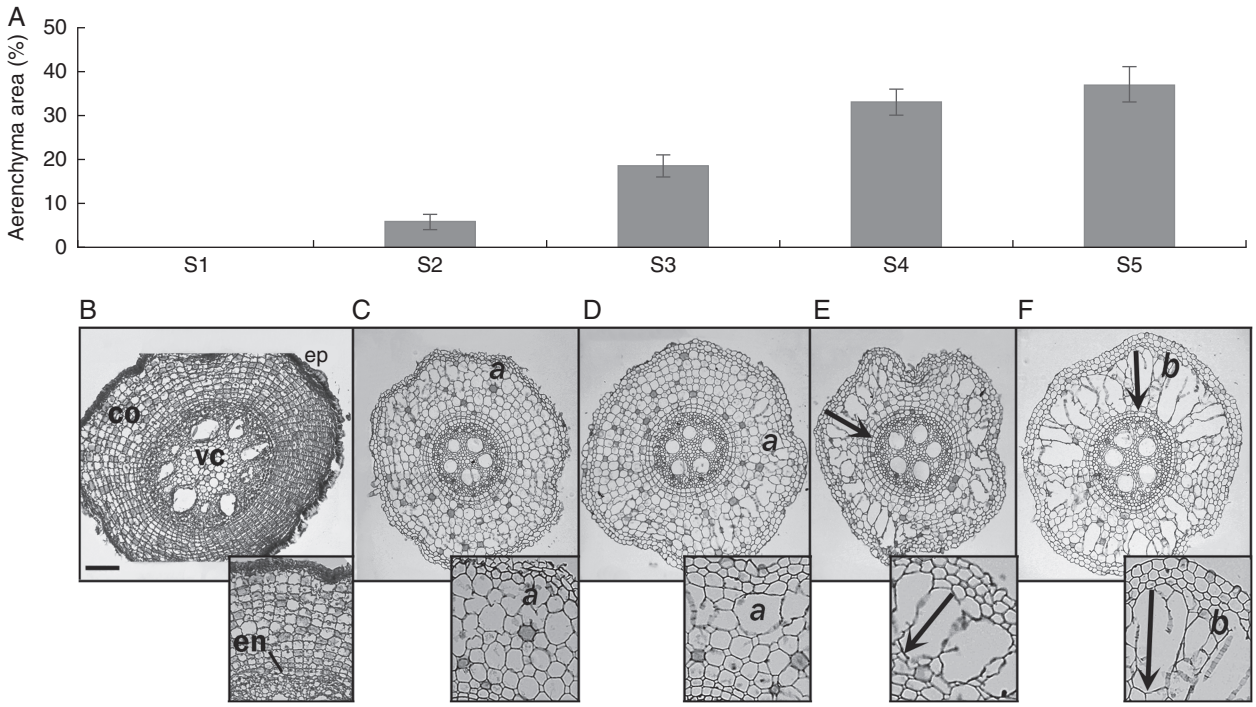

FIG. 1. Aerenchyma formation in sugarcane root from apex to 5 cm divided into 1-cm segments (S1–S5). (A) Area of aerenchyma represented as the percentage of gas spaces in root cortex ($n = 21$); bars indicate standard error. (B–F) Cross-sections of historesin-embedded root segments. (B) Root apex (S1) shows intact tissues: peripheral tissues (ep), cortex (co), endodermis (en) and vascular cylinder (vc). (C, D) Initiation of aerenchyma formation with cell wall rupture in more peripheral cells of the cortex (a in panels C and D). (E, F) Development of aerenchyma towards vascular cylinder (arrows) and fully developed aerenchyma with living cell lanes separating gas spaces (A). Scale bar = 20 μm.

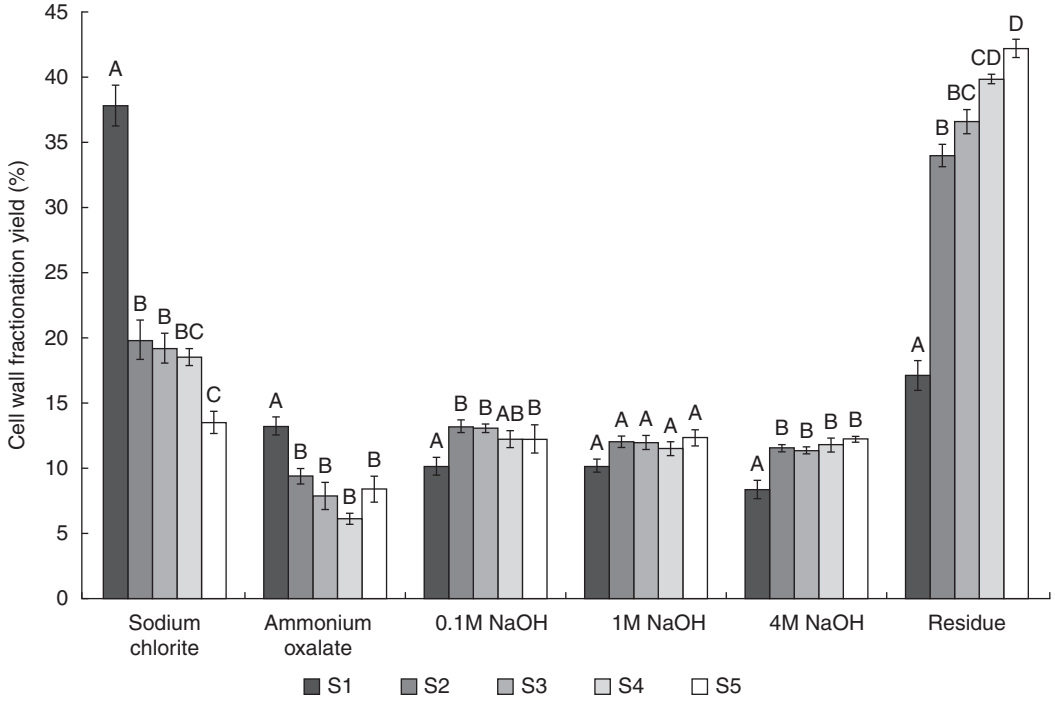

FIG. 2. Cell wall fractionation yield (percentage extracted from alcohol-insoluble residue) of root segments from apex to 5 cm divided into 1-cm segments (S1–S5). Cell walls of each segment were subjected to sequential extraction with 490 mM sodium chlorite, 0·5 % ammonium oxalate, 0·1 M NaOH, 1 M NaOH and 4 M NaOH, and material remaining after fractionation was termed the residue ($n = 5$). Bars indicate standard error. Different letters indicate significant differences.

and xylose. Arabinose, glucose and xylose were the most abundant monosaccharides present in the ammonium oxalate and NaOH fractions.

Statistically significant differences ($P < 0·05$) were observed in NaOH fractions, mostly due to glucose, xylose and galactose proportions. Glucose and galactose tended to decrease from S1 to S5, whereas xylose displayed a proportional increase towards S5 in the 0·1, 1 and 4 M NaOH fractions. These findings are indicative of the presence of arabinoxylan and/or xyloglucan. Fucose and mannose were detected in small proportions and did not differ among segments.

Remarkably, galactose decreased towards S5 in most fractions, but mainly in the ammonium oxalate and 4 M NaOH fractions. Glucose decreased in the 0·1 and 1 M NaOH fractions. These findings are suggestive of a decrease in galactan and β-glucan during root development.

Oligosaccharide profiles

We digested cell wall fractions with the glycosyl hydrolases lichenase, xylanase and xyloglucanase to evaluate the fine structures of the main hemicelluloses (β-glucan, arabinoxylan and xyloglucan). Supplementary Data Figs S1–S3 show the results of the hydrolysis of polymers present in segments 1, 3 and 5.

Supplementary Data Fig. S1 shows higher levels of β-glucan oligosaccharides in the 1 M NaOH fractions. For all extracts, no clear differences among segments were observed.

Arabinoxylan, obtained after digestion with xylanase, was mostly present in the NaOH 0·1–4 M fractions. The release of oligosaccharides characteristic of these glycans increased from S1 to S5 (Supplementary Data Fig. S2).

Xyloglucan was more abundant in the 0·1 and 1 M NaOH fractions (Supplementary Data Fig. 3). Xyloglucan from sugarcane roots displayed very complex fine structure, given the high number of peaks obtained among the limit digest oligosaccharides.

Although monosaccharide profiles suggest that β-glucan appears to decrease concomitantly with proportional increases in arabinoxylan and xyloglucan from S1 to S5, oligosaccharide analyses did not confirm this pattern. This might be explained by the fact that whereas monosaccharide analysis is exhaustive, the production of limit digest oligosaccharides is partial, reflecting the fine structural features of the walls more than a realistic quantification.

Glycome profiling

The glycome profiling data (Fig. 3) offer an alternative view of the cell wall changes during sugarcane root development. While delineating the variations in extractability of epitopes of xyloglucan, arabinoxylan and β-glucan among segments, the glycome profiles show some correlation with the changings in monosaccharide (Table 1) and oligosaccharide profiles (Supplementary Data Figs S1–S3).

Non-fucosylated xyloglucan epitopes in sugarcane roots, recognized by the XG-1 to XG-3 groups of monoclonal antibodies, were present in all segments in differing proportions, especially in all alkaline extracts. Fucosylated xyloglucan epitopes recognized by the CCRC-M84 antibody were present primarily in the 0·1 M NaOH extracts of all segments. In the more easily

TABLE 1. *Neutral monosaccharide profile in cell wall fractions of root segments from apex to 5 cm divided into 1-cm segments (S1–S5). Values indicate the percentage of each monosaccharide in each segment (n = 5) ± s.e. Letters indicate a statistical difference among segments; statistically different values are shown in bold (P < 0·05)*

		Fucose		Arabinose		Galactose		Glucose		Xylose		Mannose
Sodium chlorite	S1	1·32 ± 0·18		12·50 ± 1·77		20·28 ± 1·61		38·02 ± 3·37		**23·44 ± 1·24**	**A**	2·90 ± 0·78
	S2	0·90 ± 0·27		15·92 ± 1·32		15·71 ± 1·19		36·76 ± 4·30		**27·72 ± 1·97**	**ABC**	2·96 ± 0·75
	S3	1·33 ± 0·39		17·25 ± 1·67		15·76 ± 0·71		40·22 ± 4·04		**24·76 ± 2·58**	**ABC**	3·03 ± 0·77
	S4	0·70 ± 0·30		16·65 ± 0·61		15·71 ± 0·57		31·65 ± 1·06		**33·26 ± 1·39**	**C**	2·01 ± 0·07
	S5	1·18 ± 0·20		18·33 ± 1·36		16·94 ± 2·16		28·79 ± 1·95		**32·34 ± 2·41**	**BC**	2·38 ± 0·36
	P-value	0·44		0·07		0·12		0·10		**0·00**		0·73
Ammonium oxalate	S1	0·51 ± 0·27		12·34 ± 0·77		**12·19 ± 1·34**	**A**	49·75 ± 2·61		24·44 ± 1·42		0·73 ± 0·19
	S2	0·93 ± 0·33		12·64 ± 0·46		**7·82 ± 0·41**	**AB**	45·91 ± 2·72		26·13 ± 6·88		6·54 ± 5·90
	S3	0·50 ± 0·16		13·66 ± 0·88		**9·40 ± 1·43**	**AB**	49·86 ± 3·25		23·87 ± 6·69		0·14 ± 0·14
	S4	0·86 ± 0·36		13·59 ± 0·96		**8·46 ± 0·78**	**AB**	38·28 ± 2·25		31·36 ± 7·87		6·45 ± 6·45
	S5	0·85 ± 0·32		15·35 ± 2·30		**6·29 ± 1·22**	**B**	41·57 ± 5·01		34·64 ± 3·42		0·00 ± 0·00
	P-value	0·71		0·50		**0·01**		0·09		0·62		0·56
0·1M NaOH	S1	1·46 ± 0·98		22·10 ± 1·60		**12·02 ± 1·26**	**AB**	**21·84 ± 2·13**	**A**	**40·46 ± 4·30**	**AB**	0·23 ± 0·23
	S2	0·20 ± 0·09		23·93 ± 2·15		**13·15 ± 1·27**	**A**	**30·66 ± 1·86**	**B**	**35·78 ± 5·82**	**A**	0·26 ± 0·16
	S3	1·42 ± 1·39		22·39 ± 2·53		**11·67 ± 0·83**	**AB**	**21·92 ± 1·74**	**A**	**43·98 ± 3·77**	**AB**	0·00 ± 0·00
	S4	0·08 ± 0·08		18·92 ± 1·05		**9·00 ± 0·73**	**B**	**16·47 ± 0·37**	**A**	**55·51 ± 1·00**	**B**	0·00 ± 0·00
	S5	0·43 ± 0·14		21·27 ± 1·46		**9·14 ± 0·53**	**AB**	**16·54 ± 1·56**	**A**	**54·59 ± 2·43**	**B**	8·92 ± 8·82
	P-value	0·56		0·43		**0·02**		**<0·00**		**0·00**		0·43
1M NaOH	S1	0·37 ± 0·25		11·93 ± 1·11		**7·12 ± 0·53**	**A**	**64·30 ± 2·25**	**A**	**16·43 ± 2·78**	**A**	0·91 ± 0·78
	S2	0·01 ± 0·01		10·31 ± 0·64		**5·64 ± 0·28**	**AB**	**49·09 ± 0·94**	**B**	**34·92 ± 0·88**	**B**	0·00 ± 0·00
	S3	0·33 ± 0·33		12·39 ± 0·72		**6·11 ± 0·67**	**AB**	**36·66 ± 2·03**	**C**	**44·92 ± 1·72**	**C**	0·00 ± 0·00
	S4	0·22 ± 0·18		11·99 ± 0·79		**4·69 ± 0·55**	**B**	**35·16 ± 1·03**	**C**	**49·61 ± 0·83**	**C**	8·22 ± 8·22
	S5	0·00 ± 0·00		11·84 ± 1·17		**5·08 ± 0·57**	**AB**	**33·24 ± 1·82**	**C**	**50·60 ± 1·67**	**C**	0·00 ± 0·00
	P-value	0·59		0·56		**0·04**		**<0·00**		**<0·00**		0·45
4M NaOH	S1	0·00 ± 0·00		**7·13 ± 0·43**	**A**	**8·05 ± 0·40**	**A**	**64·32 ± 3·73**	**AB**	**18·24 ± 3·60**	**A**	2·24 ± 0·39
	S2	0·10 ± 0·09		**5·03 ± 0·45**	**AB**	**4·62 ± 0·31**	**B**	**69·64 ± 4·87**	**A**	**19·71 ± 5·07**	**A**	0·87 ± 0·54
	S3	0·00 ± 0·00		**4·80 ± 0·62**	**AB**	**3·61 ± 0·34**	**BC**	**64·71 ± 2·05**	**AB**	**25·24 ± 1·93**	**AB**	1·61 ± 0·60
	S4	0·00 ± 0·00		**4·12 ± 0·63**	**B**	**2·87 ± 0·49**	**C**	**60·34 ± 2·99**	**AB**	**31·33 ± 3·47**	**AB**	1·31 ± 0·43
	S5	0·12 ± 0·12		**6·47 ± 0·63**	**AB**	**3·68 ± 0·40**	**BC**	**52·43 ± 3·86**	**B**	**36·51 ± 3·06**	**B**	0·76 ± 0·28
	P-value	0·53		**0·00**		**<0·00**		**0·03**		**0·00**		0·20
Residue	S1	0·00 ± 0·00		**0·75 ± 0·09**	**A**	**0·75 ± 0·16**	**A**	96·38 ± 1·30		1·98 ± 0·97		0·12 ± 0·12
	S2	0·00 ± 0·00		**0·25 ± 0·10**	**B**	**0·09 ± 0·07**	**B**	98·18 ± 0·47		1·24 ± 0·53		0·21 ± 0·21
	S3	0·00 ± 0·00		**0·25 ± 0·10**	**B**	**0·19 ± 0·11**	**B**	98·48 ± 0·67		0·60 ± 0·60		0·00 ± 0·00
	S4	0·00 ± 0·00		**0·39 ± 0·05**	**AB**	**0·29 ± 0·09**	**AB**	98·52 ± 0·90		0·79 ± 0·79		0·00 ± 0·00
	S5	0·00 ± 0·00		**0·48 ± 0·09**	**AB**	**0·34 ± 0·09**	**AB**	96·90 ± 0·93		2·26 ± 0·77		0·00 ± 0·00
	P-value			**0·00**		**0·00**		0·34		0·46		0·54

released fractions (sodium chlorite and ammonium oxalate fractions), monoclonal antibodies against non-fucosylated xyloglucan epitopes displayed some binding to S1 and decreased binding to these epitopes in subsequent segments. In NaOH fractions, in general, xyloglucan epitopes were present in higher proportions and exhibited increasing trends from S1 to S5.

Xylan epitopes were recognized by monoclonal antibodies of the groups xylan-3 to 7. Among the xylan-3 antibodies, only two bound weakly (CCRC-M114 and CCRC-M116). However, for xylans-4, 5, 6 and 7, most of the antibodies of each class displayed a peak at S3, decreased signal at S4, and peaked again at S5. These four groups of monoclonal antibodies showed quite similar patterns of variation.

Two monoclonal antibodies detecting polysaccharides containing 1,3-β linkages were used (LAMP, specific for 1,3 β-glucan, and BG1, specific for 1,3;1,4 β-glucan, here termed β-glucan). Only BG1 bound to sugarcane cell wall extracts. β-Glucan epitopes occurred in all fractions and did not show any significant change from S1 towards S5.

Homogalacturonan backbone-2 monoclonal antibodies bound weakly to polysaccharides in sodium chlorite and even more weakly to polymers present in the ammonium oxalate fractions. As expected, these epitopes were absent in the alkaline extracts, which would remove the methyl esters. Antibodies against de-esterified homogalacturonans (Homogalacturonan-1 group) were weakly detected in the sodium chlorite, 0·1 M NaOH and 1 M NaOH fractions.

In general, the abundance of pectic arabinogalactan epitopes, specifically those recognized by RG-I/AG group of monoclonal antibodies, was significantly higher in 0·1, 1 and 4 M NaOH extracts. The pattern of variation of the rhamnogalacturonan-I/arabinogalactan monoclonal antibodies indicated that the corresponding polymers peaked at S3 and S5.

Immunofluorescence labelling

Based on glycome profiling (Fig. 3), we selected nine monoclonal antibodies representing every class of polysaccharide within sugarcane cell walls for fluorescence microscopy visualization of S1, S3 and S5. We chose the antibodies on the basis of the intensity observed in the glycome profiles as well as on preliminary tests performed with a few antibodies in each group (data not shown). We chose for further observations the

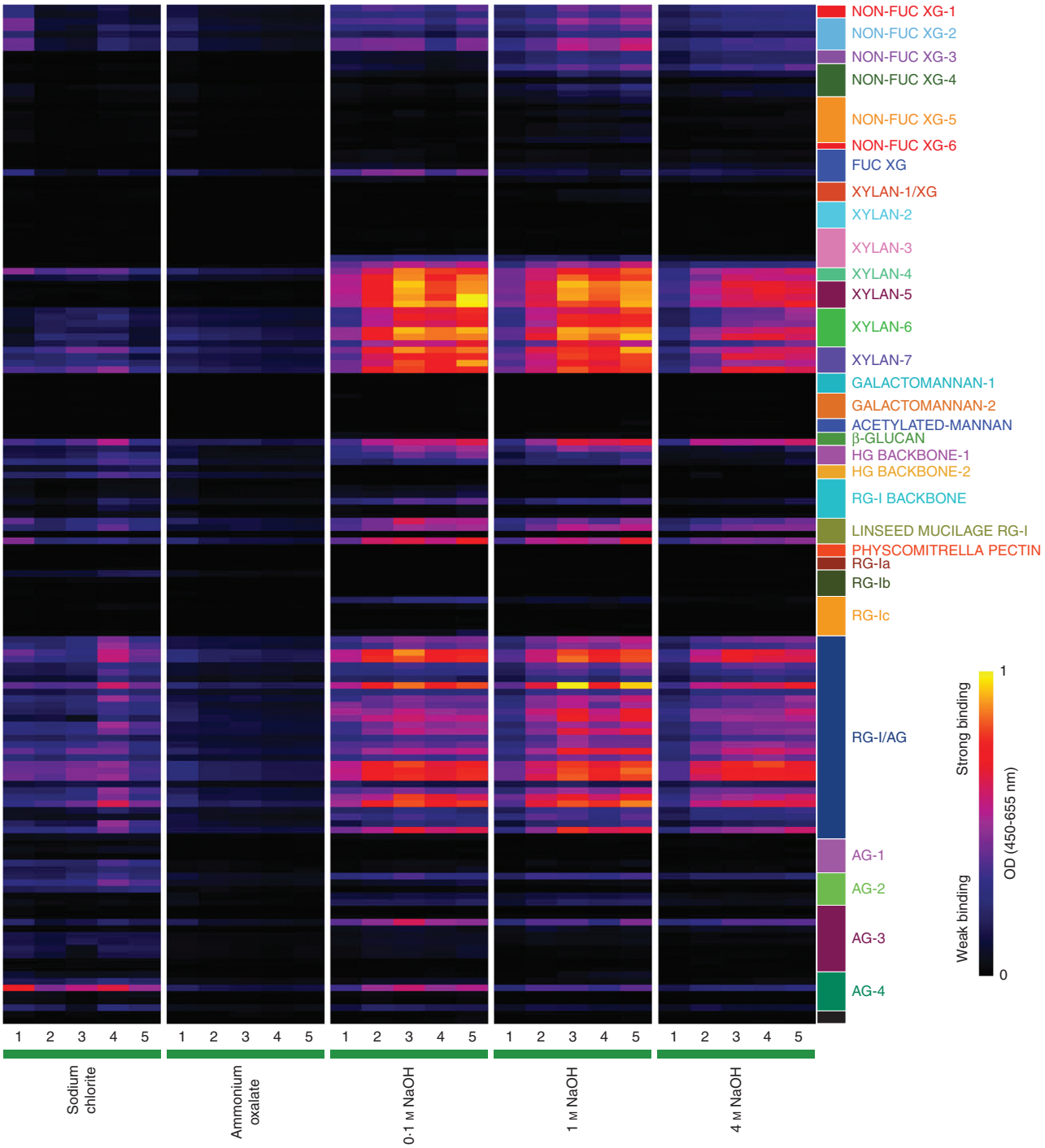

FIG. 3. Glycome profiling of cell wall extracts of root segments from root apex to 5 cm divided into 1-cm segments (numbered 1–5). Cell walls of each segment were subjected to sequential extraction with 490 mM sodium chlorite, 0·5 % ammonium oxalate, 0·1 M NaOH, 1 M NaOH and 4 M NaOH. Solubilized extracts were screened for an array of plant glycan-directed monoclonal antibodies (Pattathil *et al*., 2010, 2012) using ELISA. Absorbances are represented according to the colour key on the right. Antibodies are grouped according to the polysaccharides predominantly recognized (coloured boxes): non-fucosylated xyloglucan (NON-FUC-1-6), fucosylated xyloglucan (FUC XG), xylan/xyloglucan (XYLAN-1/XG), XYLAN-2-7, GALACTOMANNAN-I-2, ACETYLATED MANNAN, β-GLUCAN, homogalacturonan backbone (HG BACKBONE-1 and -2), rhamnogalacturonan backbone (RGI BACKBONE), linseed mucilage rhamnogalacturonan (LINSEED MUCILAGE RG-I), *Physcomitrella* pectin, rhamnogalacturonan-I (RG-Ia, b and c), rhamnogalacturonan-I/arabinogalactan (RG-I/AG), arabinogalactan (AG-1 to -4).

antibodies that presented more consistent binding throughout the cortex.

Regarding the non-fucosylated xyloglucan, CCRC-M95 monoclonal antibody cross-reacted with xyloglucan in metaxylem and with peripheral tissues (epidermis, exodermis and sclerenchymatous cylinder) in all segments (Fig. 4). In S5, this monoclonal antibody stained cell walls of cortical cells slightly more intensely, suggesting that the epitope for this monoclonal antibody became available as a result of cell wall changes that took place during root development. The monoclonal antibody used to label fucosylated xyloglucan (CCRC-M84) showed fluorescence only in the outer walls of the epidermis, preserving the same pattern in all segments (data not shown).

We chose two antibodies for detection of xylans in the root tissues: (1) CCRC-M154 (XYLAN-4), which binds specifically to the arabinosyl side-chains of arabinoxylans (Schmidt *et al*., 2015); and (2) CCRC-M138 (XYLAN-6), which binds specifically to a xylan backbone epitope consisting of at least five unmodified xylosyl residues [information available at WallMabDB (http://wallmabdb.net)].

In sugarcane roots, the monoclonal antibody staining xylan-4 (CCRC-154) displayed strong binding to the walls of all cells of the root section in all segments (Fig. 5 D–F). The monoclonal antibody specific for longer stretches of unmodified xylan backbone (CCRC-M138) labelled mostly exodermis and the sclerenchymatous cylinder, endodermis, early metaxylem and pith, but not the epidermis (Fig. 5 J–L). In this case, labelling fluorescence increased slightly, particularly for the vascular cylinder, from S1 to S3, and only weak label was seen in the cortex. The results with CCRC-M138 suggest that more unbranched xylans are present in the vascular system going from S1 to S5. A slight increase in binding of CCRC M138 to the cortex cell walls was also observed (Fig. 5 J–L), indicating the possibility of some increased deposition of unbranched xylans or an increase in the accessibility of unmodified xylan backbone epitopes to this monoclonal antibody during the development of the sugarcane root.

BG1 (a monoclonal antibody that recognizes β-glucan) bound to all cell walls in S1 (Fig. 6D), and the staining started to fade specifically in cortex cells at S3 (Fig. 6E). In S5, BG1 shows practically no more labelling in the cortex, while its fluorescence remains strong in the peripheral tissues and vascular cylinder (Fig. 6F).

It was noticeable that the disappearance of BG1 binding followed a centripetal pattern.

We observed five different patterns after using antibodies against pectins.

(1) CCRC-M23, which targets rhamnogalacturonan-I, showed no staining (data not shown) despite the cross-reactivity of this monoclonal antibody in the glycome profile.

(2) In cortex cells, the homogalacturonan backbone-binding monoclonal antibody CCRC-M38 cross-reacted markedly with cell wall junctions in all segments (Fig. 7).

(3) The rhamnogalacturonan-I/arabinogalactan monoclonal antibody CCRC-M80 strongly labelled all cell walls, except for those surrounding gas spaces (Fig. 8). In S1, speckled labelling of cytoplasmic content was observed closer to the inner face of the walls. This labelling was seen in S3, but in this case it was distributed throughout the cytoplasm and in alternating cells. However, this staining pattern was no longer present in S5. Together, these observations suggest that some deposition of

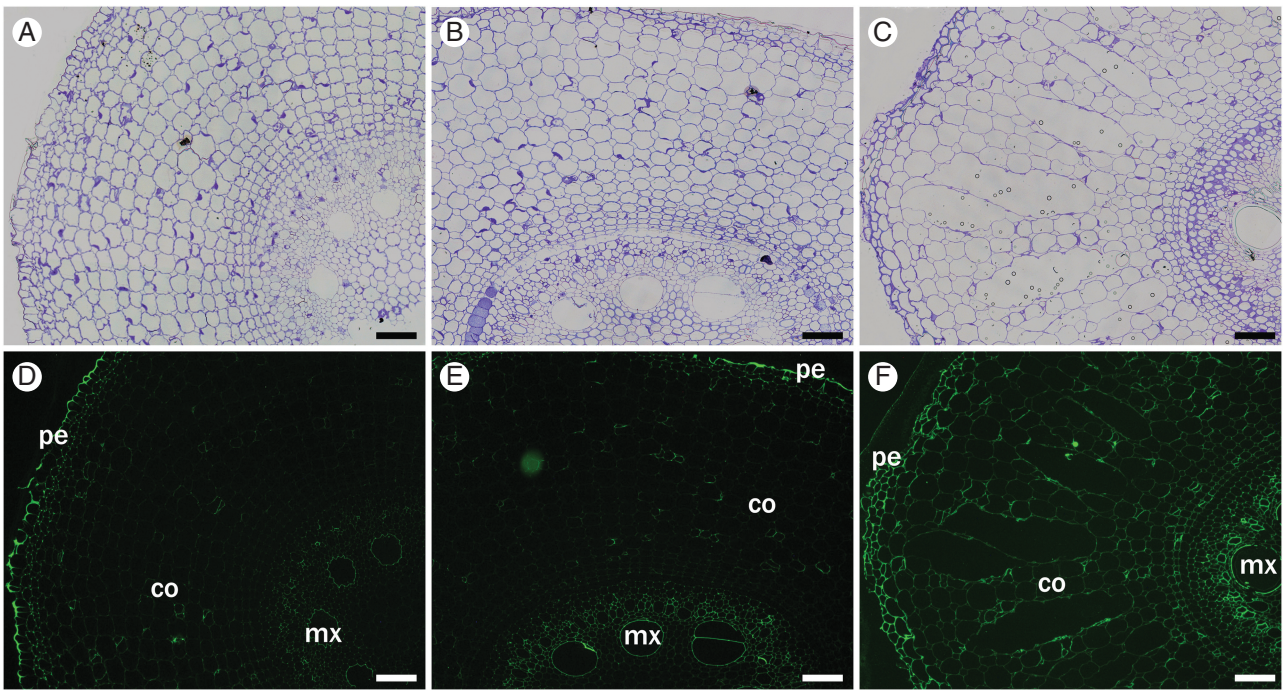

FIG. 4. Immunofluorescence labelling of cross-sections of root segments S1 (A, D), S3 (B, E) and S5 (C, F) using non-fucosylated xyloglucan-directed antibody (CCRC-M95). Labelling appears in metaxylem (mx), epidermis (pe) and other peripheral tissues. Little binding of the antibody to cortex (co) in all segments, although intensity increases in S5 (D–F). Controls (A–C) were stained with toluidine blue. Scale bars = 100 μm.

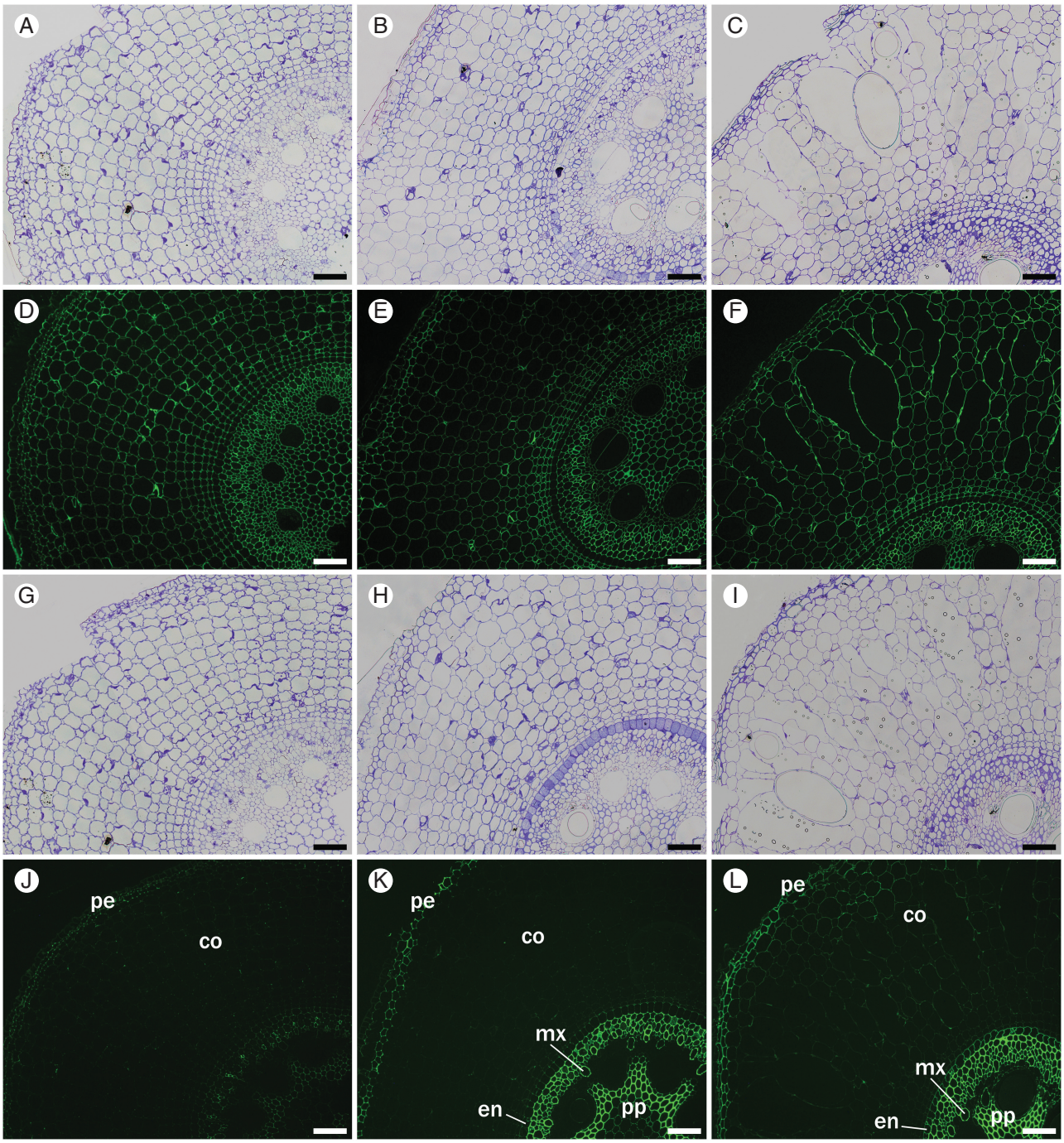

FIG. 5. Immunofluorescence labelling of cross-sections of root segments S1 (A, D, G, J), S3 (B, E, H, K) and S5 (C, F, I, L) using xylan-4- and xylan-6-directed antibodies (CCRC-M154 and CCRC-M138, respectively). (D–F) CCRC-M154 labelled all cell walls in every segment. CCRC-M138 binds to peripheral tissues (pe), such as exodermis and the sclerenchymatous cylinder, as well as endodermis (en), early metaxylem (mx) and pith (pp); epidermis and metaxylem are not labelled, and only slight fluorescence is seen in the cortex (co). Controls were stained with toluidine blue for CCRC-M154 (A–C) and CCRC-M138 (G–I). Scale bars = 100 μm.

rhamnogalacturonan-I/arabinogalactan might occur during the early phases of development.

(4) JIM14, which binds to arabinan, mostly showed speckled labelling in the sclerenchymatous cylinder and vascular cylinder, remaining constant throughout the period of aerenchyma formation (Fig. 9C).

(5) The monoclonal antibody JIM19 labelled arabinogalactan proteins in the cytoplasm, adjacent to cell walls, mainly in S5. It is noticeable that staining was lower around the aerenchyma cavities, where the cells were dying (Fig. 9D).

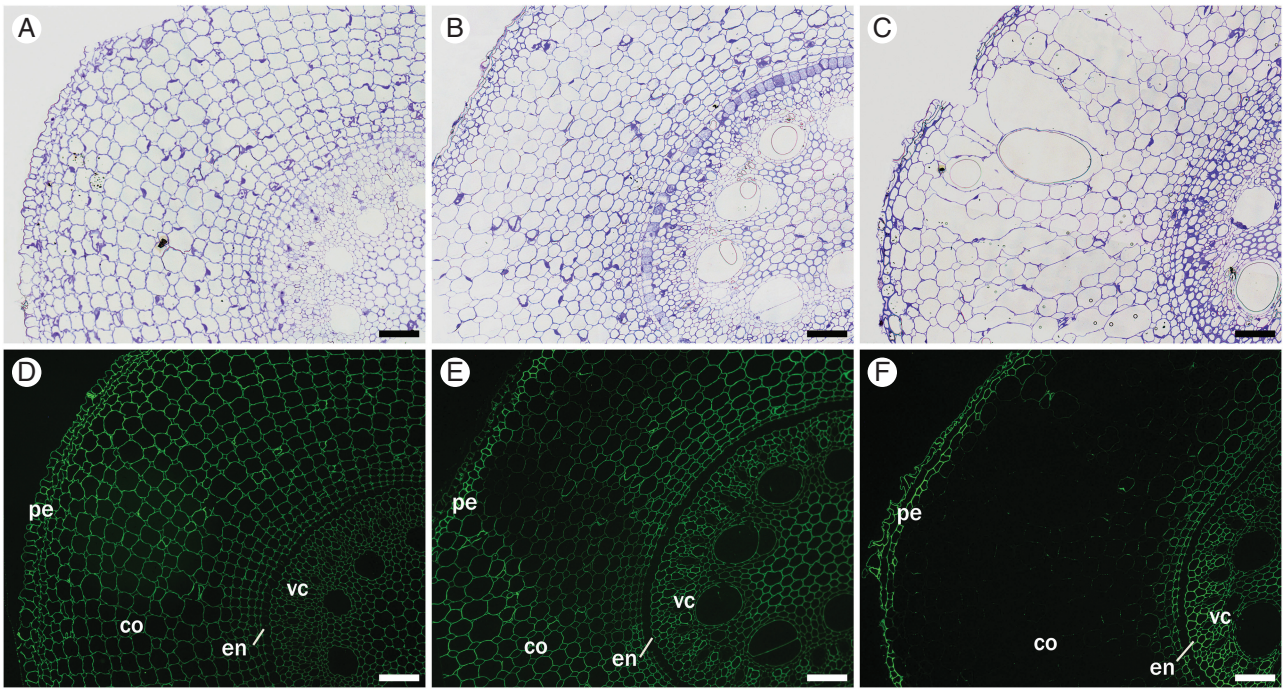

FIG. 6. Immunofluorescence labelling of cross-sections of root segments S1 (A, D), S3 (B, E) and S5 (C, F) using β-glucan-directed antibody (BG1). Labelling in sections initiates in all cell walls in S1, fades at the cortex in S3, and practically disappears from the cortex in S5, although it persists in peripheral tissues (pe) (epidermis, exodermis and sclerenchymatous cylinder) and vascular cylinder (vc). Endodermis (en) is not labelled in all sections. Controls (A–C) were stained with toluidine blue. Scale bar = 100 μm.

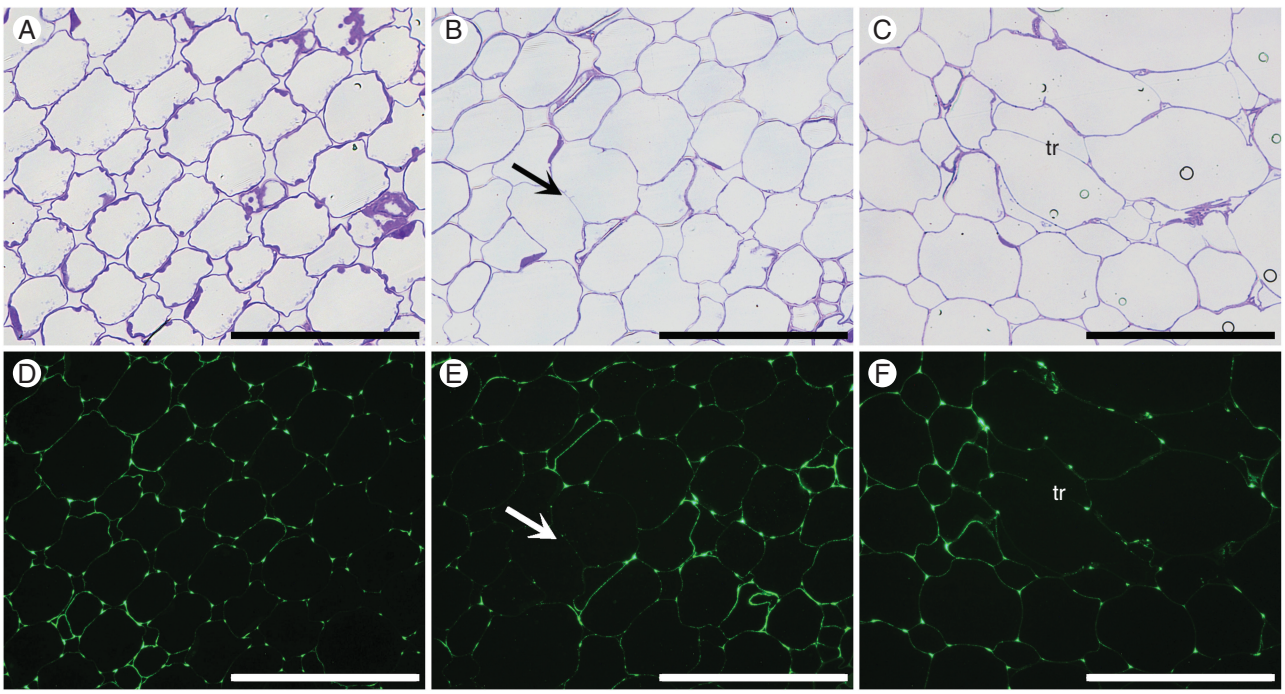

FIG. 7. Immunofluorescence labelling of cross-sections of the cortex tissue of root segments S1 (A, D), S3 (B, E) and S5 (C, F) using de-esterified backbone-directed antibody (CCRC-M38). Labelling is more prominent in cell intersections (triangular junctions) in S1 and decreases towards S5, but can still be seen in cell walls (tr, trabeculae) in regions surrounding aerenchyma. Scale bar = 100 μm.

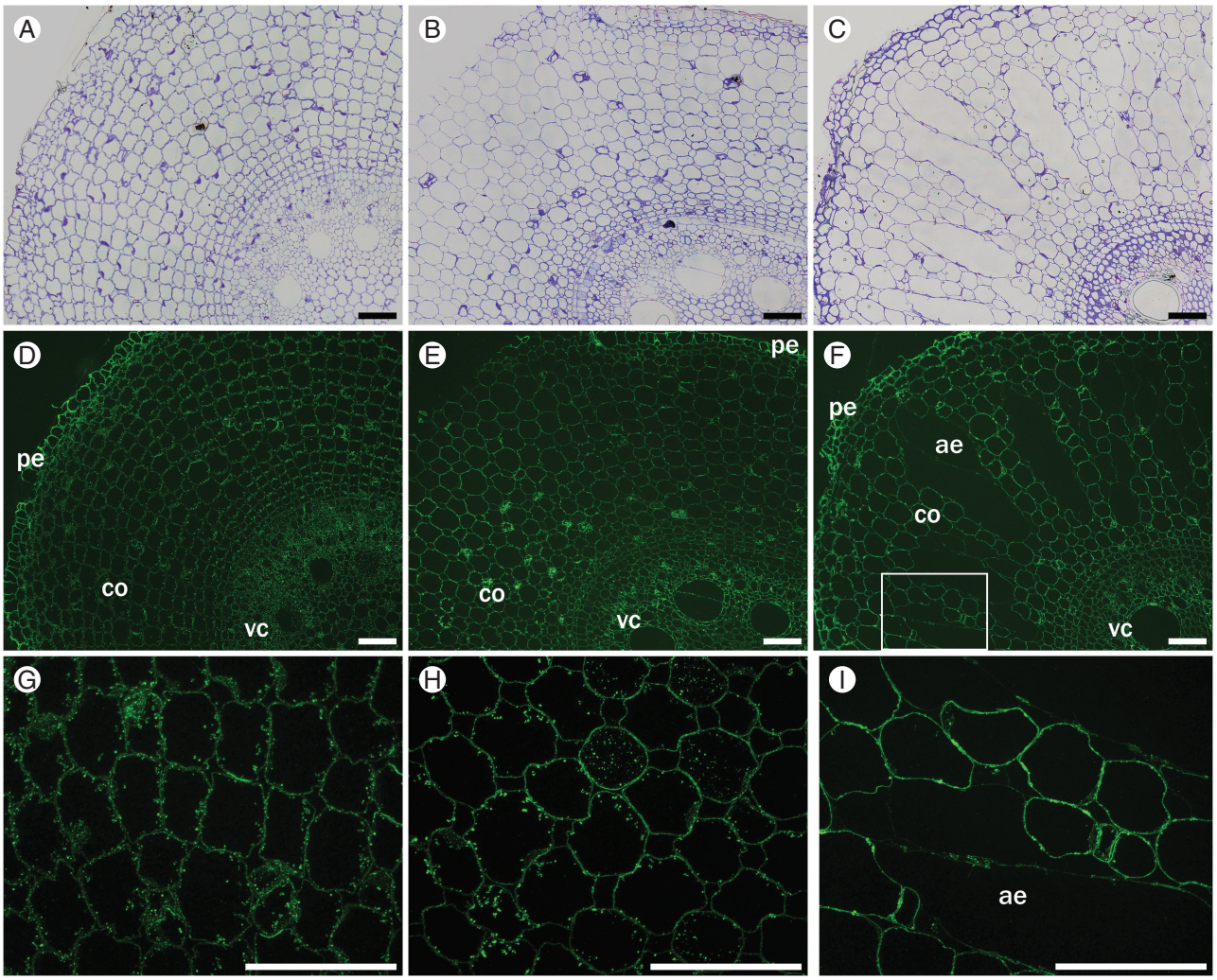

FIG. 8. Immunofluorescence labelling of transverse cross-sections from root segments S1 (A, D, G), S3 (B, E, H) and S5 (C, F, I) using the pectic arabinogalactan-directed antibody CCRC-M80. This antibody labels all cell walls in all segments (pe, peripheral tissues; co, cortex; vc, vascular cylinder) (D–F), except for those forming trabeculae inside the aerenchyma (ae). In S1, this antibody also shows labelling of cytoplasmic content closer to inner-facing walls in the cortex (G); labelling is weaker in S3 (H) and absent in S5 (I). The rectangle in (F) is an enlargement of the region shown in I. Controls (A–C) were stained with toluidine blue. Scale bar = 100 μm.

Immunogold labelling

We used this technique with the aim of detecting the polysaccharides left after the modification of cell walls during aerenchyma formation in the cortex. Thus, only S4 and S5 sections were used. Xylans were visualized using the monoclonal antibody CCRC-M154 at later stages of aerenchyma formation in cell walls surrounding the gas spaces (Fig. 10A, B). β-Glucan was located (detected by the monoclonal antibody BG1) in the inner facing walls of living cells (Fig. 10C), but not detectable in cell walls forming aerenchyma composites, i.e. walls from dead cells. De-esterified homogalacturonan, as detected by the monoclonal antibody CCRC-M38, was scarce, only being found next to a junction of neighbouring cells, at this point restricted to a space delimited by a thin cell wall (Fig. 10D). To help visualization of the gold particles, they have been digitally coloured in red in Fig. 10 (Supplementary Data Fig. S5 shows the original figures).

DISCUSSION

In some tissues, cell walls can undertake deep modifications, participating in cell or tissue differentiation and changing the fate of entire organs (Roberts *et al*., 2002; Grandis *et al*., 2014; Tavares *et al*., 2015). Here we studied aerenchyma formation in sugarcane roots from a cell wall perspective. We characterized the aerenchyma in sugarcane roots during its development, focusing on the events associated with changes in cell wall composition, polysaccharide fine structure, morphology and some of the ultrastructure.

At the tissue level, light microscopy and X-ray microtomography showed that aerenchyma formation in sugarcane roots progresses centripetally. It first appears at the second centimetre from the root tip (S2) with a few larger intercellular spaces, occupying ~6 % of the cortical area (Fig. 1C and Supplementary Data Video). Gas spaces are restricted to the cortex, which is a thick layer of cells beneath the three outer cell layers: epidermis,

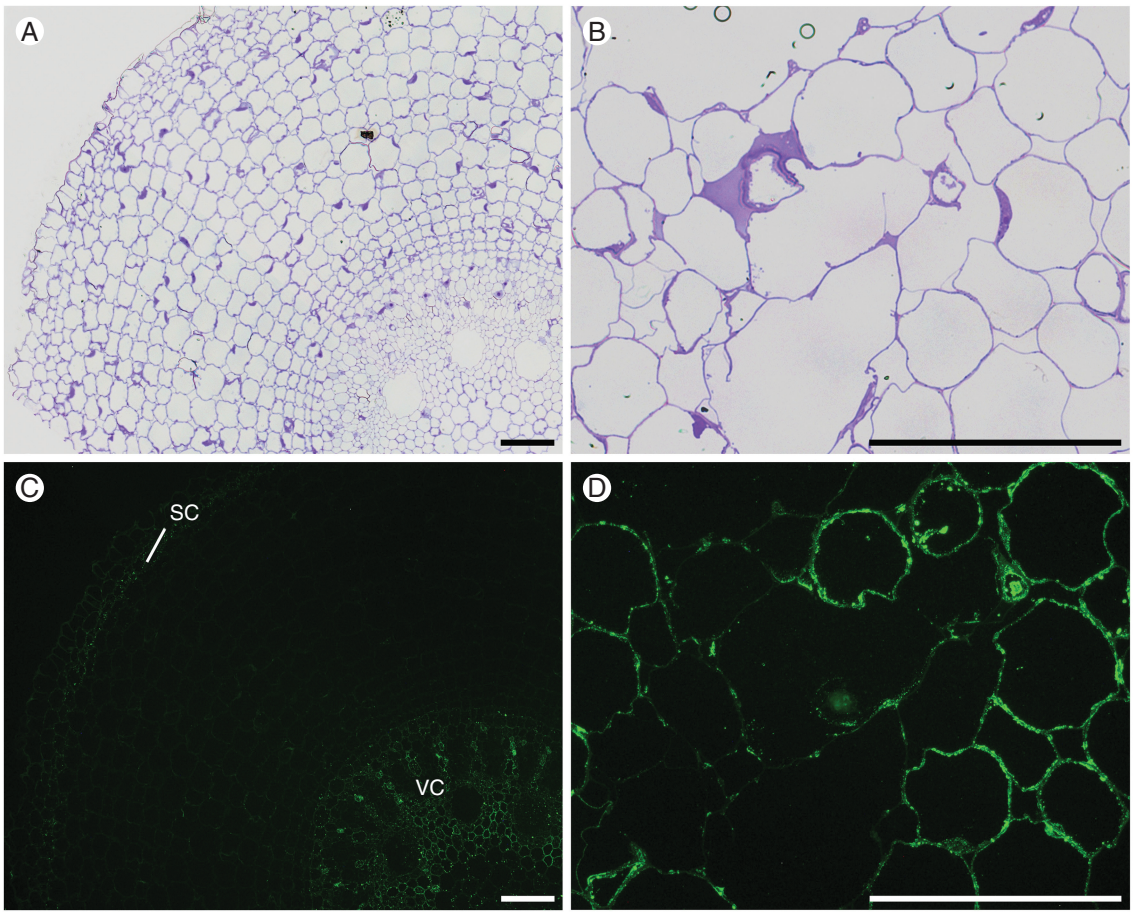

FIG. 9. Immunofluorescence labelling of cross-sections of root segments using arabinogalactan-directed antibodies JIM14 (S5; A, C) and JIM19 (S1; B, D). (C) the speckled binding pattern of JIM14 monoclonal antibody, labelling cytoplasmic contents of cells from the sclerenchymatous cylinder (sc) and vascular cylinder (vc) in S1. (D) JIM19 binds to cytoplasmic material and cell walls of S5, but binding weaker to walls surrounding the aerenchyma. Controls (A, B) were stained with toluidine blue. Scale bar = 100 μm.

exodermis and the sclerenchymatous cylinder, whose cell walls become thicker as roots develop (Rebouillat *et al.*, 2009). These layers of intact cells are thought to be an impermeable barrier to radial O_2 loss, enabling its diffusion from the shoot to the root tip through aerenchyma (Colmer, 2003).

Sugarcane aerenchyma becomes fully developed at S5 (4–5 cm from the root tip), where gas spaces occupy an average of 37 % of the cortex area (Fig. 1 and Supplementary Data Video). We found that the gas spaces are not linearly continuous, but interspaced with patches of intact tissue. In the regions where aerenchyma is present, radial trabeculae are formed by scrambled cell wall material left after programmed cell death (to be described elsewhere).

Below we discuss the modifications of cell walls associated with the events taking place in the cortex during aerenchyma development.

Cell wall modifications during aerenchyma formation

The attack on pectins is an early step in aerenchyma formation (Gunawardena et al., 2001*b*). Pectins are important in cell walls due to the role they play in cell adhesion, expansion and porosity of the cell wall (Baron-Epel *et al.*, 1988; Ridley et al., 2001; Yamauchi *et al.*, 2013). During fruit ripening, for instance, homogalacturonan present in the middle lamella can be depolymerized. Therefore, the presence of pectin-degrading enzymes, as well as accumulation of their transcripts, is important for fruit softening (Harker *et al.*, 1997; Rose et al., 1998; Brummell, 2006).

In aerenchyma formation, enzyme activities and gene expression related to pectin modifications have been detected during the development of aerenchyma in maize, suggesting that a similar mechanism exists in roots (Bragina et al., 2003; Rajhi et al., 2011).

In the present work, we showed that cell expansion takes place in the cortex of sugarcane roots at the same time as part of the tissue loses its integrity. This occurs after cell wall separation takes place. These findings are consistent with the slight decrease in staining of cell walls by the homogalacturonan monoclonal antibody (CCRC-M38) around the opening gas spaces (Fig. 7). The removal of pectins, probably homogalacturonan, a debranched pectin present mainly in the middle lamella (Knox, 1992), is more evident in the immunogold data,

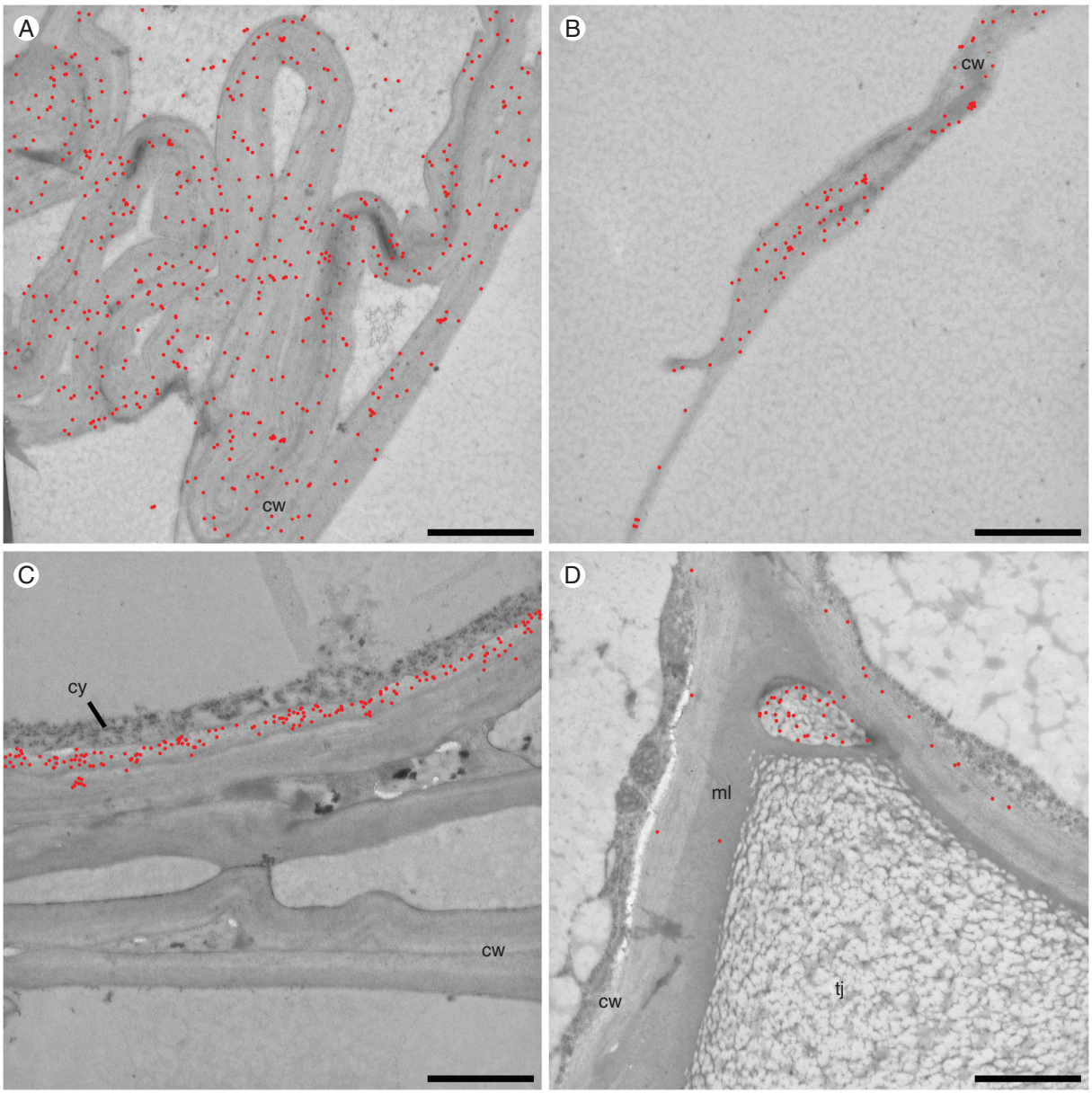

FIG. 10. Immunolocalization with colloidal gold in transmission electron microscopy. (A, B) Location of xylans demonstrated with antibody CCRC-M154 along all the collapsed walls (A) and in smaller quantities even in debris of extracellular material (B). (C) Staining of β-glucan with BG1 antibody in the inner portion of the cell wall of a living cell, adjacent to the collapsed walls, from where β-glucan has disappeared. (D) Staining of de-esterified homogalacturnonans (CCRC-M38) in cell walls of living cells and intercellular material in the triangular junction region. Gold particles are highlighted in red for better visualization. cw, cell wall; cy, cytoplasm; ml, middle lamella; tj, triangular junction. Scale bars = 10 µm.

in which a residual amount of the polymer remains in the walls after aerenchyma formation (Fig. 10D). Gunawardena *et al.* (2001*b*) obtained similar results for maize aerenchyma using monoclonal antibodies for both esterified and de-esterified pectins (JIM7 and JIM5, respectively).

In sugarcane roots, we observed that the levels of galactose decreased from S1 to S2 in ammonium oxalate fractions (Table 1), indicating that some galactan degradation may have occurred. However, this was not corroborated by use of the monoclonal antibody CCRC M80, which binds to arabinogalactan. The reason why galactan would be degraded before aerenchyma formation is unknown, but it is possible to speculate that it could be related to increasing cell wall porosity during the process. A possible explanation for the modifications in pectins of sugarcane root tips is that these changes could be part of a mechanism involving a step in preparation for hemicellulose and cellulose modifications later during the completion of aerenchyma formation.

Removal of β-glucan from the cortex coincides with aerenchyma formation

The loss of the β-glucan detectable by BG1 monoclonal antibody using immunofluorescence occurs exclusively in the root cortex, being consistent with aerenchyma formation (Fig. 6). However, despite the fact that estimation of β-glucan by hydrolysis with lichenase suggests a slight decrease in β-glucan levels towards S5, β-glucan detection did not disappear completely from the roots. In fact, β-glucan staining remained consistent in the cells of the epidermis and the vascular system of the root (Fig. 6). This is probably the reason why detection of β-glucan by the BG1 monoclonal antibody is maintained in the glycome profile. Our results suggest that the endogenous lichenases are exclusively expressed in the cells of the cortex, but not in other cells, at least within the first 5 cm of the roots.

A different pattern of β-glucan deposition was noticed by immunogold labelling, with which it is located on the inner layer of the wall, facing the plasma membrane (Fig. 10C). A similar pattern was observed in maize coleoptile and barley (Willats *et al*., 2001; Tretheway and Harris, 2002). Willats *et al*. claim that this pattern is the result of late deposition of β-glucan, while Tretheway and Harris believe it is related to the removal of β-glucan from specific regions.

One possible explanation for the removal of β-glucan from the cortex cell walls in sugarcane roots is that β-glucan might work as a scaffold for the assembly of the walls during development and its subsequent removal when wall complete differentiation. Carpita and Gibeaut (1993) proposed the hypothesis that β-glucan and arabinoxylan chains are associated, and evidence for such interaction was obtained by Izydorczyk and MacGregor (2000).

Indeed, β-glucan is believed to be a transition polysaccharide, synthesized in elongating tissues and degraded as elongation ceases (Carpita, 1996; Kim *et al*., 2000). In this case, the removal of β-glucan from the cell walls could be a post-developmental event, not directly related to aerenchyma development. However, we cannot rule out the hypothesis that aerenchyma formation in sugarcane is indirectly related to the degradation of β-glucan in some cortex cells. Its removal may allow modifications of other polymers of the cell wall matrix in the presence of the proper enzymes.

Xyloglucan, arabinoxylan, cellulose and lignin may physically support the composite formed by aerenchyma

Relatively little xyloglucan is present in the cell walls of sugarcane roots (Fig. 3 and Supplementary Data Fig. S3). However, it has been hypothesized by De Souza *et al*. (2013) and Buckeridge *et al*. (2015) that xyloglucan may play a role in sugarcane cell wall architecture, possibly by holding macrofibrils together.

During the formation of aerenchyma in maize roots, Rajhi *et al*. (2011) found increased expression of xyloglucan transglycosylase-hydrolase, an enzyme capable of remodelling xyloglucan chains and affecting cell expansion in association with aerenchyma formation. In other systems, such as fruit ripening and cell wall storage mobilization, xyloglucan may be subjected to changes, including depolymerization (Rose and Bennett, 1999; Buckeridge, 2010; Grandis *et al*., 2014). In sugarcane roots, xyloglucan monoclonal antibodies showed stronger binding to some cell walls during aerenchyma development (Figs 3 and 4), suggesting that xyloglucan modifications could contribute to remodelling of cell walls in the cortex. The possible rearrangement of xyloglucan is observed concomitantly with stronger binding to the walls of S1–S5. This suggests that xyloglucan might bind to cellulose and also to arabinoxylan, participating in the formation of the cell wall composite visualized at the end of aerenchyma formation.

When the monoclonal antibody M154 was used, a behaviour similar to that of xyloglucan was observed for arabinoxylan immunolabelling (Fig. 5), i.e. a slight increase in staining towards S5. This increase in staining may result from either the increased deposition of arabinoxylan or removal of xylan modifications (e.g., acetylation) that lead to greater antibody access to its epitope in the walls.

Previous reports assessed the requirement of xylanase in the formation of aerenchyma in maize. Although enzyme activity towards arabinoxylan was detected in flooded adventitious roots of maize (Bragina *et al*., 2001, 2003), its transcript was downregulated in maize root cortex after flooding. The present study does not corroborate previous suggestions of arabinoxylan hydrolysis during aerenchyma development. Immunogold localization of arabinoxylan in sugarcane roots indicates that xylans detected by the monoclonal antibody CCRC-M154 remain in the cortex cell walls after aerenchyma formation, including the regions around gas spaces (Fig. 10 A, B). The behaviour of arabinoxylan during aerenchyma formation in sugarcane supports the hypothesis that this polysaccharide, together with xyloglucan, is one of the main compounds responsible for the features of the composites formed during development.

Cellulase activity has been pointed out as a hallmark of aerenchyma formation. Activity of this enzyme was measured by the increased carboxymethylcellulase activity (He *et al*., 1992; Bragina *et al*., 2003). Furthermore, Rajhi *et al*. (2011) separated root maize cortex from the vascular cylinder and found some cellulase-associated gene expression in the cortex. The present study shows increasing yields of residues after cell wall fractionation (mainly composed of cellulose; >96 % glucose) from S1 to S5 (Fig. 2, Table 1). Since in our analyses glucose derived not only from the cortex but also from the vascular cylinder, it is likely that part of the cellulose accumulation observed is related to xylogenesis.

We cannot discard the hypothesis that there is some enzyme action towards cellulose microfibrils of the cortex. For example, during avocado fruit ripening, O'Donoghue *et al*. (1994) found that cellulase attacks the amorphous regions of cellulose microfibrils. A rise in crystallinity was observed, denoting the fact that cellulases might increase resistance to further attack on the microfibrils.

The fact that total lignin contents in root segments do not change during aerenchyma development (Supplementary Data Fig. S4) suggests that the modifications of the cell walls of the cortex are probably not related to complete cell wall degradation. This is corroborated by the fact that arabinoxylan displays little change during the process. It can also be suggested that the lignin–arabinoxylan architectural feature (if any) might be preserved in the composites formed in the aerenchyma. Altogether, the walls that form aerenchyma seem to lose their

natural features after cells collapse, forming wrinkled structures rich in xyloglucan, arabinoxylans, cellulose and possibly some lignin.

Possible roles of cell walls in aerenchyma and prospects for biotechnology

The developmental steps undertaken by the cells of the cortex of sugarcane roots include cell expansion, cell separation, cell death and, at the same time, mechanical modifications of cell walls that lead to the formation of composites. The latter form an inner layer that surrounds the gas spaces within the roots. Here we report the events taking place in the cortex cell walls; we found that, whereas pectins and β-glucan are altered, xyloglucan, arabinoxylan, cellulose and possibly lignin become part of cell wall composites that form the inner side of the aerenchyma gas spaces. This structure can increase the strength of the aerenchyma structure and create gas spaces at the same time as maintaining root mechanical properties. Such composite features have been observed in rice pulp hemicelluloses (Mobarak *et al*., 1973) and storage xyloglucans (Lima *et al*., 2003). Lima *et al*. found that the addition of only 1 % of hemicelluloses (xyloglucan or galactomannan) to a paper pulp (i.e. to cellulose) was capable of increasing the mechanical properties of paper by 30 %. Also, Gáspár *et al*. (2005) found that corn hemicellulose (probably rich in arabinoxylan) increased the tensile strength of compostable starch-based plastics. At the same time, it increased water absorption by these composites.

Thus, we hypothesize that the modification of cell walls during lysigenous aerenchyma formation, culminating in the formation of a cell wall composite, may keep the mechanical strength of the trabecular structure formed in the cortex of sugarcane roots.

By learning how sugarcane can modify its walls, our discoveries highlight ways of learning about genes encoding transcription factors and enzymes that could be related to this self-modifying system. At the same time as we find out more about aerenchyma formation in roots of grasses, we could also use such mechanisms for designing new materials for biorefinery and improve second-generation bioenergy production from sugarcane and other grasses.

SUPPLEMENTARY DATA

Supplementary data are available online at www.aob.oxfordjournals.org and consist of the following. Video: a general perspective of the experiment displaying a series of pictures (2970) and microtomographic sequences of sugarcane root segments S1–S5. Figure S1: oligosaccharide profiles of cell wall extracts of root segments treated with lichenase (for detection of β-glucan). Trisaccharide (a), tetrasaccharide (b) and pentasaccharide (c). Figure S2: oligosaccharide profiles of cell wall extracts of root segments (S1, S3 and S5) treated with xylanase (for detection of xylans). Xylose (a), xylobiose (b), xylotriose (c) and arabinosylated oligosaccharides (d).

Figure S3: oligosaccharide profiles of cell wall extracts of root segments (S1, S3 and S5) treated with xyloglucan endoglucanase (XEG, for detection of xyloglucan). Figure S4: lignin contents in root segments (S1–S5) of sugarcane. Data are percentages of lignin in the segment. Figure S5: immunolocalization with colloidal gold in transmission electron microscopy. Location of arabinoxylans with the antibody CCRC-M154 along all the collapsed walls and in smaller quantities in the intercellular content (A, B).

ACKNOWLEDGEMENTS

This work was partly funded by the Instituto Nacional de Ciência e Tecnologia do Bioetanol – INCT do Bioetanol (FAPESP 2008/57908-6 and CNPq 574002/2008-1) and of the Centro de Processos Biológicos e Industriais para Biocombustíveis – CeProBIO (FAPESP 2009/52840-7 and CNPq 490022/2009-0). DCCL (FAPESP 2010/12833-9), AG (FAPESP2010/17070-3) and AG BEPE-Italy (FAPESP2013/0159-0) and a Fapesp Research Grant (2010/17104-5). Also supported in part by a grant from the U.S. National Science Foundation (IOS-0923992) to MGH. The generation of the CCRC series of plant cell wall glycan-directed monoclonal antibodies used in this work was supported by the U.S. National Science Foundation Plant Genome Program (DBI-0421683 and IOS-0923992).

LITERATURE CITED

Abiko T, Kotula L, Shiono K, Malik A, Colmer TD, Nakazono M. 2012. Enhanced formation of aerenchyma and induction of a barrier to radial oxygen loss in adventitious roots of *Zea nicaraguensis* contribute to its waterlogging tolerance as compared with maize (*Zea mays* ssp. *mays*). *Plant, Cell and Environment* **35**: 1618–1630.

Avci U, Pattathil S, Hahn MG. 2012. Immunological approaches to plant cell wall biomass characterization: immunolocalization of glycan epitopes. In: Himmel ME. ed. *Biomass conversion methods and protocols. Methods in molecular biology*, Vol. **908**. New York: Humana Press, 73–82.

Baron-Epel O, Gharyal PK, Schindler M. 1988. Pectins as mediators of wall porosity in soybean cells. *Planta* **175**: 389–395.

Begum MK, Alam MR, Islam MS. 2013. Adaptive mechanisms of sugarcane genotypes under flood stress condition. *World Journal of Agricultural Sciences* **1**: 56–64.

Bragina TV, Martinovich LI, Rodionova NA, Bezborodov AM, Grineva GM. 2001. Ethylene induced activation of xylanase in adventitious roots of maize as a response to the stress effect of root submersion. *Applied Biochemistry and Microbiology* **37**: 722–725.

Bragina TV, Rodionova NA, Grinieva GM. 2003. Ethylene production and activation of hydrolytic enzymes during acclimation of maize seedlings to partial flooding. *Russian Journal of Plant Physiology* **50**: 794–798.

Brummell DA. 2006. Cell wall disassembly in ripening fruit. *Functional Plant Biology* **33**: 103–119.

Buckeridge MS. 2010. Seed cell wall storage polysaccharides: models to understand cell wall biosynthesis and degradation. *Plant Physiology* **154**: 1017–1023.

Buckeridge MS, Santos WD, Tiné MS, de Souza AP. 2015. The cell wall architecture of sugarcane and its implication to cell wall recalcitrance. In: Lam E, Carrer H, Silva JA. eds. *Compendium of bioenergy plants: sugarcane*. Boca Raton: CRC Press, 31–50.

Carpita NC. 1996. Structure and biogenesis of the cell walls of grasses. *Annual Review of Plant Physiology and Molecular Plant Biology* **47**: 445–476.

Carpita NC, Gibeaut DM. 1993. Structural models of primary cell walls in flowering plants: consistency of molecular structure with the physical properties of the cell wall during growth. *The Plant Journal* **3**: 1–30.

Colmer TD. 2003. Long-distance transport of gases in plants: a perspective on internal aeration and radial oxygen loss from roots. *Plant, Cell & Environment* **26**: 17–36.

Damásio ARL, Ribeiro LFC, Ribeiro LF, *et al.* 2012. Functional characterization and oligomerization of a recombinant xyloglucan-specific endo-β-1,4-

glucanase (GH12) from *Aspergillus niveus*. *Biochimica et Biophysica Acta* **1824**: 461–467.

DeMartini JD, Pattathil S, Avci U, *et al.* 2011. Application of monoclonal antibodies to investigate plant cell wall deconstruction for biofuels production. *Energy and Environmental Science* **4**: 4332–4339.

Drew MC, He CJ, Morgan PW. 2000. Programmed cell death and aerenchyma formation in roots. *Trends in Plant Science* **5**: 123–127.

Evans DE. 2003. Aerenchyma formation. *New Phytologist* **161**: 35–49.

Gáspár M, Benko ZS, Dogossy G, Réczey K, Czigány T. 2005. Reducing water absorption in compostable starch-based plastics. *Polymer Degradation and Stability* **90**: 563–569.

Grandis A, de Souza AP, Tavares EQP, Buckeridge MS. 2014. Using natural plant cell wall degradation mechanisms to improve second generation bioethanol. In: McCann MC, Buckeridge MS, Carpita NC, eds. *Plants and bioenergy*. New York: Springer, 211–230.

Gunawardena AH, Pearce DM, Jackson MB, Hawes CR, Evans DE. 2001*a*. Characterisation of programmed cell death during aerenchyma formation induced by ethylene or hypoxia in roots of maize (*Zea mays* L.). *Planta* **212**: 205–214.

Gunawardena A, Pearce DM, Jackson MB, Hawes CR, Evans DE. 2001*b*. Rapid changes in cell wall pectic polysaccharides are closely associated with early stages of aerenchyma formation, a spatially localized form of programmed cell death in roots of maize (*Zea mays* L.) promoted by ethylene. *Plant, Cell and Environment* **24**: 1369–1375.

Harker FR, Redgwell RJ, Hallet IC, Murray SH, Carter G. 1997. Texture of fresh fruit. *Horticultural Reviews* **20**: 121–124.

He C, Finlayson SA, Drew MC, Jordan WR, Morgan PW. 1996. Ethylene biosynthesis during aerenchyma formation in roots of maize subjected to mechanical impedance and hypoxia. *Plant Physiology* **112**: 1679–1685.

He CJ, Morgan P, Drew MC. 1992. Enhanced sensitivity to ethylene in nitrogen- or phosphate-starved roots of *Zea mays* L. during aerenchyma formation. *Journal of Plant Physiology* **98**: 137–142.

He CJ, Drew M, Morgan PW. 1994. Induction of enzymes associated with lysigenous aerenchyma formation in roots of *Zea mays* during hypoxia or nitrogen starvation. *Plant Physiology* **105**: 861–865.

Izydorczyk MS, MacGregor AW. 2000. Evidence of intermolecular interactions of beta-glucans and arabinoxylans. *Carbohydrate Polymers* **41**: 417–420.

Justin SHFW, Armstrong W. 1991. Evidence for the involvement of ethylene in aerenchyma formation in adventitious roots of rice (*Oryza sativa* L.). *New Phytologist* **118**: 49–62.

Kawase M. 1979. Role of cellulase in aerenchyma development in sunflower. *American Journal of Botany* **66**: 183–190.

Kim JB, Olek AT, Carpita NC. 2000. Plasma membrane and cell wall exo-β-D-glucanases in developing maize coleoptiles. *Plant Physiology* **123**: 471–485.

Knox JP. 1992. Cell adhesion, cell separation and plant morphogenesis. *Plant Journal* **2**: 137–141.

Kong Y, Zhou G, Yin Y, Xu Y, Pattathil S, Hahn M. 2011. Molecular analysis of a family of *Arabidopsis* genes related to galacturonosyl transferases. *Plant Physiology* **155**: 1791–1805.

Lima DU, Chaves RO, Buckeridge MS. 2003. Seed storage hemicelluloses as wet-end additives in papermaking. *Carbohydrate Polymers* **52**: 367–373.

Mobarak F, El-Ashawy AE, Fahmy Y. 1973. Hemicelluloses as additives in papermaking. 2. The role of added hemicelluloses and hemicellulose *in situ* on paper properties. *Cellulose Chemistry Technology* **7**: 325–335.

Moreira-Vilar FC, Siqueira-Soares RC, Finger-Teixeira A, *et al.* 2014. The acetyl bromide method is faster, simpler and presents best recovery of lignin in different herbaceous tissues than klason and thioglycolic acid methods. *PLoS ONE* **9**: e110000. doi:10.1371/journal.pone.0110000.

O'Donoghue EM, Huber DJ, Timpa JD, Erdos GW, Brecht JK. 1994. Influence of avocado (*Persea americana*) Cx-cellulase on the structural features of avocado cellulose. *Planta* **194**: 573–584.

Pattathil S, Avci U, Baldwin D, *et al.* 2010. A comprehensive toolkit of plant cell wall glycan-directed monoclonal antibodies. *Plant Physiology* **153**: 514–525.

Pattathil S, Avci U, Miller JS, Hahn MG. 2012. Immunological approaches to plant cell wall and biomass characterization: glycome profiling. In: Himmel M. ed. *Biomass conversion: methods and protocols. Methods in molecular biology*, Vol. **908**. New York: Humana Press, 61–72.

Rajhi I, Yamauchi T, Takahashi H, *et al.* 2011. Identification of genes expressed in maize root cortical cells during lysigenous aerenchyma formation using laser microdissection and microarray analyses. *New Phytologist* **190**: 351–368.

Rebouillat J, Dievart A, Verdeil JL, *et al.* 2009. Molecular genetics of rice root development. *Rice* **2**: 15–34.

Ridley BL, O'Neill MA, Mohnen D. 2001. Pectins: structure, biosynthesis, and oligogalacturonide-related signaling. *Phytochemistry* **57**: 929–967.

Roberts JA, Elliott KA, Gonzalez-Carranza Z. 2002. Abscission, dehiscence, and other cell separation processes. *Annual Review of Plant Biology* **53**: 131–158.

Rose JKC, Bennett AB. 1999. Cooperative disassembly of the cellulose-xyloglucan network of plant cell walls: parallels between cell expansion and fruit ripening. *Trends in Plant Science* **4**: 176–183.

Rose JKC, Hadeld KA, Labavitch JM, Bennett AB. 1998. Temporal sequence of cell wall disassembly in rapidly ripening melon fruit. *Plant Physiology* **117**: 345–361.

Saab IN, Sachs MM. 1996. A folding-induced xyloglucan endotransglycosylase homolog in maize is responsive to ethylene and associated with aerenchyma. *Journal of Plant Physiology* **112**: 385–391.

Saeman JF, Harris EE, Kline AA. 1945. Quantitative saccharification of wood and cellulose. *Industrial and Engineering Chemistry, Analytical Edition* **17**: 35–37.

Seago JL Jr, Marsh LC, Stevens KJ, Soukup A, Votrubová O, Enstone DE. 2005. A re-examination of the root cortex in wetland flowering plants with respect to aerenchyma. *Annals of Botany* **96**: 565–579.

Schmidt D, Schuhmacher F, Geissner A, Seeberger PH, Pfrengle F. 2015. Automated synthesis of arabinoxylan-oligosaccharides enables characterization of antibodies that recognize plant cell wall glycans. *Chemistry-A European Journal* **21**: 5709–5713.

Schussler EE, Longstreth D. 2000. Changes in cell structure during the formation of root aerenchyma in *Sagittaria lancifolia* (Alismataceae). *American Journal of Botany* **87**: 12–19.

De Souza AP, Leite DCC, Pattathil S, Hahn MJ, Buckeridge MS. 2013. Composition and structure of sugarcane cell wall polysaccharides: implications for second-generation bioethanol production. *BioEnergy Research* **2**: 564–579.

De Souza AP, Kamei CLA, Torres AF, *et al.* 2015. How cell wall complexity influences saccharification efficiency in *Miscanthus sinensis*. *Journal of Experimental Botany* **66**: 4351–4365.

Tavares EQP, de Souza AP, Buckeridge MS. 2015. How endogenous plant cell-wall degradation mechanisms can help achieve higher efficiency in saccharification of biomass. *Journal of Experimental Botany* **66**: 4133–4143.

Tetsushi H, Karim MA. 2007. Flooding tolerance of sugarcane in relation to growth physiology and root structure. *South Pacific Studies* **28**: 9–22.

Trethewey JAK, Harris PJ. 2002. Location of (1 3)- and (1 3),(1 4)-beta-D-glucans in vegetative cell walls of barley (*Hordeum vulgare*) using immunogold labelling. *New Phytologist* **154**: 347–358.

Visser EJ, Bögemann GM. 2006. Aerenchyma formation in the wetland plant *Juncus effusus* is independent of ethylene. *New Phytologist* **171**: 305–314.

Willats WG, McCartney L, Mackie W, Knox JP. 2001. Pectin: cell biology and prospects for functional analysis. *Plant Molecular Biology* **47**: 9–27.

Yamauchi T, Shimamura S, Nakazono M, Mochizuki T. 2013. Aerenchyma formation in crop species: a review. *Field Crops Research* **152**: 8–16.

Zhu X, Pattathil S, Mazumder K, Brehm A, Hahn MG, Dinesh-Kumar SP *et al.* 2010. Virus-induced gene silencing offers a functional genomics platform for studying plant cell wall formation. *Molecular Plant* **3**: 818–833.